JOURNAL OF MATERIALS SCIENCE 18 (1983) 3265–3280

A study of the ageing behaviour of a cobalt based implant alloy

R. N. J. TAYLOR,* R. B. WATERHOUSE
Department of Metallurgy and Materials Science, University of Nottingham, UK

The ageing characteristics of a commercial CoCrMoC alloy were investigated using optical and electron microscopy. Only one phase, the $M_{23}C_6$ type carbide, was positively identified by X-ray and electron diffraction after treatments between 650 and 1175° C for times up to 188 h. Three types of precipitation mechanism were found to operate, the mode of nucleation being dependent upon temperature. At low (< 925° C) temperatures the carbide precipitated on intrinsic stacking faults (h c p cobalt) probably by means of Suzuki segregation. A discontinuous reaction also occurred at grain boundaries in order to assist precipitation, resulting in a lamellar "pearlitic" morphology. At temperatures in excess of 925° C the carbide nucleated and grew on dislocations. This was a result of the increased thermodynamic stability of the f c c cobalt matrix, and the decreasing stacking fault density. Particle coarsening and spheroidisation and agglomeration of the lamellae were also evident. Sharp decreases in ductility associated with ageing precluded any commercial benefit of this type of treatment, despite substantial increases in hardness.

1. Introduction

Cobalt based superalloys were originally developed from dental alloys, for use in the gas turbine industry, but they have been largely superseded by nickel base alloys due to the innovation of dispersion hardening [1]. However, mainly because of the recent advances in medicine and surgical technique, the biomedical applications as implant materials have now become the main usages of the CoCrMoC alloys, due to their excellent corrosion resistance.

The main strengthening mechanism of most of the cobalt superalloys is the presence of carbide second phases [2, 3]. The size, distribution, morphology and extent of these phases are important in determining the effect on mechanical properties. A number of complex carbide reactions and intermetallics may occur in this type of alloy, as well as the allotropic transformation of the cobalt matrix between the face centred cubic (f c c) and the hexagonal close packed (h c p) structures.

The early research [4–11] carried out in this alloy was primarily aimed at the high temperature strength properties and therefore a complete investigation of its ageing behaviour had not been carried out.

NACA research [4–7] studied the HS 21 alloy in its wrought form. A solution treatment of 1230° C for 24 h [7] was found to dissolve completely the residual carbides, but a large increase in grain size also resulted. Clemow and Daniell [12] studied the solution treatment behaviour of a CoCrMoC alloy at temperatures in excess of 1160° C. The dissolution rate of residual $M_{23}C_6$, (where M = Co, Cr, Mo), carbides was dependent upon the alloy composition, the temperature, and time of the solution treatment, and the heating rate. Observed transformations to M_6C and σ-phase also complicated the issue. Temperatures in excess of 1210° C and times > 1 h were required for satisfactory treatments, in general.

Weeton and Signorelli [6, 11], Clauss and Weeton [4, 5] and Clauss *et al.* [7] performed ageing and isothermal treatments between 650 and 1065° C for 5 min to 72 h on wrought HS 21 after a solution treatment of 1230° C for 72 h. The ageing operation gave rise to intragranular,

*Present address: AWRE, Aldermaston, Reading, UK.

0022–2461/83 $03.00 + .12

"feathery", precipitation at temperatures in excess of 650° C. Striations were also visible and were attributed to slip lines resulting from the thermal shock of the quench [11]. Agglomeration of the precipitate at grain boundaries was also seen after extensive times at the higher temperatures. At 1065 and 955° C the reaction was complete after 1 to 2 h, but continued to increase up to 72 h at 815° C.

Isothermal treatments gave rise to a lamellar morphology at the grain boundaries, plus a star-shaped interdendritic precipitate. Air cooling of the aged specimens also showed this phenomenon [7, 11]. The occurrence of the lamellar morphology in a series of alloys was investigated in some detail by Weeton and Signorelli [6]. The effects of treatment temperature and chemical composition were not conclusively determined. Fletcher and Elsea [13] also noted this morphology in the X-40 alloy, but only when a slow cooling rate or a high nitrogen content was present.

Spheroidization of the lamellae at 1065 and 955° C took place after approximately 2 h, in a similar fashion to iron carbide in pearlitic steels treated for long periods below the eutectoid temperature.

Several workers [8–10] have investigated the ageing behaviour of the cast alloy. Only an interdendritic precipitate was recorded, with no striations or lamellar precipitation being evident.

The phases present have been reported as being M_6C, $M_{23}C_6$, M_7C_3 and the intermetallic σ-phase. Stain etching and heat tinting, which are dependent upon chemical composition, cannot be considered conclusive in this system due to the variability of the percentage of each solute in the carbides with heat treatment. Weeton and Signorelli [6] used X-ray diffraction on the ground powders after annealing them at 815° C for 30 min. However, this would, itself, cause further precipitation, as shown in this paper and their results must be interpreted carefully. Indications were given that the $Cr_{23}C_6$ and σ-phases were present, with the possibility of the M_6C and Cr_7C_3 carbides.

Other authors [10, 12] electrolytically extracted the second phases prior to X-ray diffraction. Unfortunately, weak and overlapping lines occur with the possible phases present although the removal of the cobalt matrix is beneficial, and the changing chemical composition results in variations in the lattice parameter, making positive identification difficult. Using the extraction method, Lane and Grant [10] proposed the transformation $M_7C_3 \rightarrow M_{23}C_6$ in the cast alloy on ageing, at ~ 800° C, and Clemow and Daniell [12] the transformation $M_{23}C_6 \rightarrow M_6C$ at ~ 1210° C.

In utilizing transmission electron microscopy (TEM), Vander Sande *et al.* [14] verified the presence of the $M_{23}C_6$ carbide in the solution treated and aged material, by electron diffraction. Although σ-phase was indicated from stain etching results, none could be found in the thin foils prepared.

Some doubt therefore remains as to the exact nature of the ageing phases and any transformations which may occur.

2. Experimental procedure

The material was received as investment cast blocks in the production solution treated condition. This consisted of holding the alloy at 1220° C for 1.5 h in a vacuum furnace, and gas quenching. The chemical analysis is given in Table I. These blocks were sectioned into test coupons of dimensions 10 mm x 10 mm x 5 mm. A typical microstructure is shown in Fig. 1, showing a coarse dendritic structure.

The ageing operations were carried out in a tube furnace with a purified dried argon atmosphere. A water quench followed every treatment. For the very short ageing times a salt bath furnace was used, so that instantaneous heating could be assumed from the greater rate of heat transfer. This was only available up to 1000° C. Excessive corrosion was not found despite earlier reports [7, 11].

Prior to metallographic examination, 1 mm was ground off the surface. This was to remove any decarburized or deformed material, since the sectioning of the blocks may possibly have induced an allotropic transformation within the metastable f c c cobalt matrix.

An electrolytic etch in 5% nitric acid in

TABLE I Chemical composition of the Co–Cr–Mo alloy

Element	wt%
Chromium	28.3
Molybdenum	5.4
Carbon	0.26
Manganese	0.66
Iron	0.39
Nickel	0.12
Cobalt (balance)	62.3

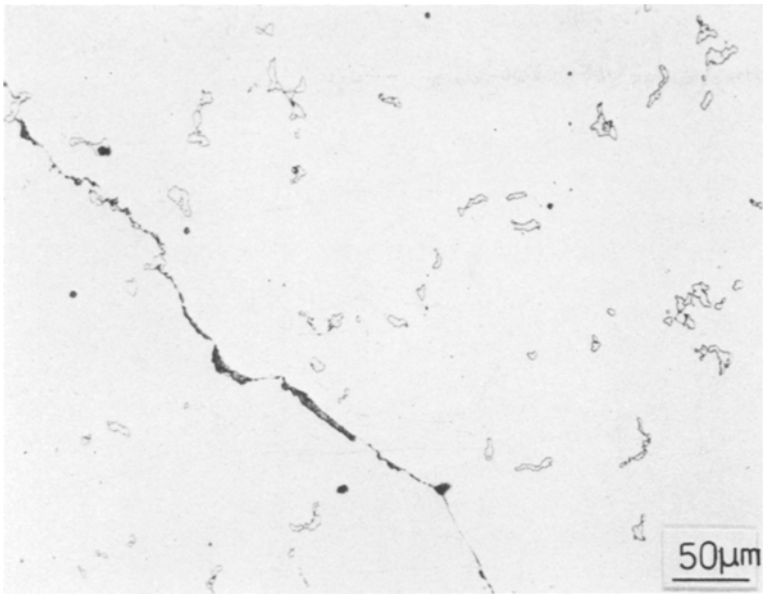

Figure 1 Production solution heat treated material. Coarse grained structure with inter-dendritic and grain boundary carbides.

methanol proved effective. In conjunction with the Cambridge 600 Stereoscan and Jeol 35C scanning electron microscopes, energy dispersive X-ray analysis (EDXA) was available for qualitative chemical analysis. X-ray diffraction studies were performed using CrK_α radiation. The second phases were electrolytically extracted in 10% H_2SO_4 in methanol [15] and filtered in sintered glass crucibles onto glass fibre filter papers. Direct analysis of the papers, after washing and drying, was possible in a diffractometer. Identification was made by comparison with the ASTM Powder Diffraction File and with the results tabulated by Donachie and Kriege [15].

Gravimetric analysis of the filtered residue was attempted in order to obtain the weight percentages of the second phases present. However, the errors involved rendered the validity of the results questionable and they are therefore not presented.

Thin foils were prepared for use in a Philips 301 electron microscope in four, sometimes five, stages. The rapid work hardening characteristics of the material restricted the amount of grinding possible. Initially the coupons were ground manually to ~ 500 μm. Spark machining was considered the only viable method of producing 3 mm diameter discs. Manual polishing followed down to ~ 200 to 300 μm, and final thinning was achieved using a jet electrolytic polisher. The most satisfactory electrolyte proved to be that used by Yukawa and Sato [16], Table II. The large grain size necessitated the examination of large areas of thin material for a complete investigation, but the chemical inhomogeneities made this very difficult. A final treatment of ion beam bombardment was required with the majority of the perforated foils in order to produce acceptable regions for examination.

3. Results and discussion

3.1. Qualitative analysis

X-ray diffraction on the electrolytically extracted second phase particles resulted in the positive identification of the presence of the $M_{23}C_6$ type carbide (where M = Co, Cr, Mo). The lattice parameter, a, was determined as 1.065 nm. No other second phase was detected in the thirteen specimens tested. The existence of only one carbide was supported by the electron diffraction observations.

In previous studies conducted on this and similar alloy systems, a variety of phases have been reported. These include the M_7C_3 [10, 17], M_6C [12, 16, 18] and MC [16, 19] carbides, intermetallic [11, 12, 14] as well as the $M_{23}C_6$ [9–12, 14, 16–19] carbide.

The discrepancies with these authors may be

TABLE II Composition of polishing electrolyte

(ml)
750 diethylene glycol
248 conc. sulphuric acid
10 water
3 conc. hydrochloric acid

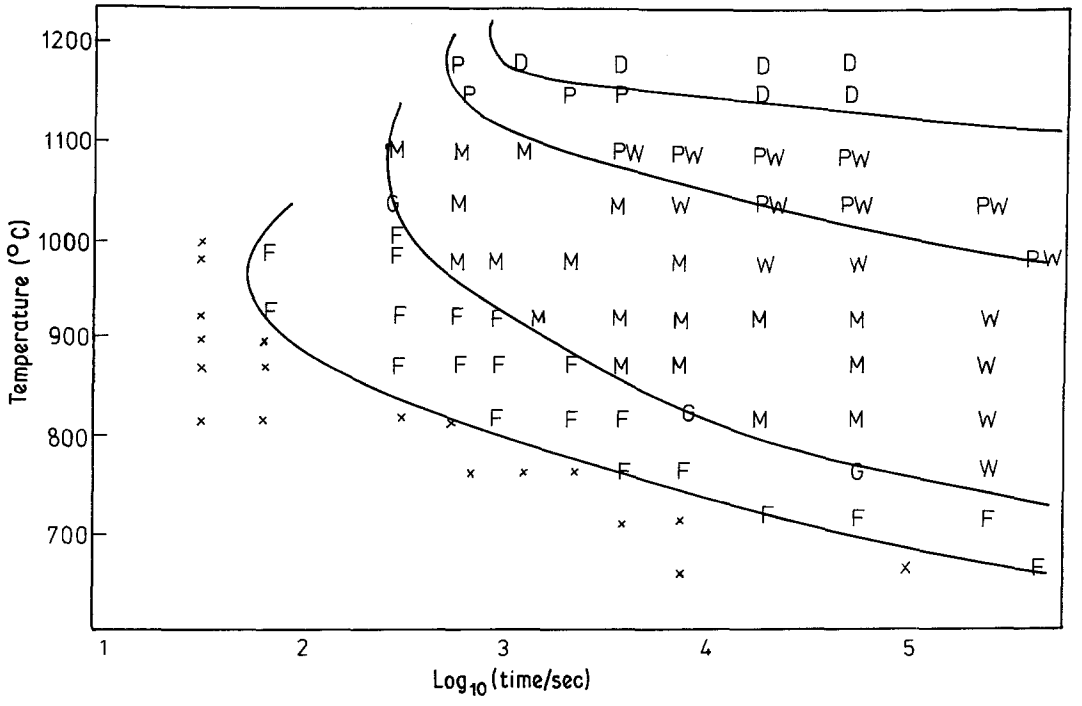

Figure 2 Time–temperature–precipitation (TTP) diagram on ageing production solution heat treated material. Key: X no new precipitate; F feathery, interdendritic precipitate, and lamellar structure at grain boundaries; G blocky grain boundary phase; M change in morphology; W orientation effects in the matrix phase; P no lamellar structure; PW spheroidized, agglomerated lamellae; D dissolution apparent.

explained. Stain etching and heat tinting [6, 9, 11, 12, 14] cannot be regarded as definitive tests in this and related alloy systems because of the varying chemical composition of the carbide during heat treatment. This was clearly indicated by energy dispersion X-ray analysis (EDXA). The residual carbides were rich in chromium and molybdenum, but deficient in cobalt with respect to the matrix. The precipitating secondary carbides showed the same trend, particularly as the ageing time and temperature increased.

In Goldschmidt's study [20] on the $M_{23}C_6$ type carbides occurring in some steels, it was found that chromium could be replaced by up to 30% iron in the complex fcc structure. Any further increase demanded the addition of tungsten to stabilize the lattice, since too much space became available, and tungsten, being larger, could fill the gaps. The interatomic distances between cobalt and iron, and between tungsten and molybdenum are approximately the same, and therefore it is reasonable to assume that same arguments apply to this system. Hence the $M_{23}C_6$ carbide may contain substantial amounts of cobalt and molybdenum without any change in lattice structure, which supports the EDXA and X-ray diffraction results.

Clemow and Daniell [12] proposed the transformation from $M_{23}C_6$ to M_6C at 1210° C, but the ageing times were too brief in this study at 1175° C to record the changes and Lane and Grant [10] proposed the M_7C_3 to $M_{23}C_6$ reaction on heat treatment of an as-cast alloy and so this, once again, was not applicable.

3.2. Metallography

A time–temperature–precipitation (TTP) diagram, Fig. 2, was constructed on the basis of the metallographic changes observed on ageing, since no phase change was detected and the kinetics of the reaction were not determined.

Two types of response were readily apparent on ageing at temperatures $\geqslant$ 650° C. Within the grains, a fine precipitate was observed, which increased in number and size with time and temperature, Figs. 3 to 6. This concurred with the early NACA research [9–11] on the ageing behaviour of the as-cast Vitallium alloy. The inhomogeneous distribution was a result of residual coreing from the investment casting operation, and became increas-

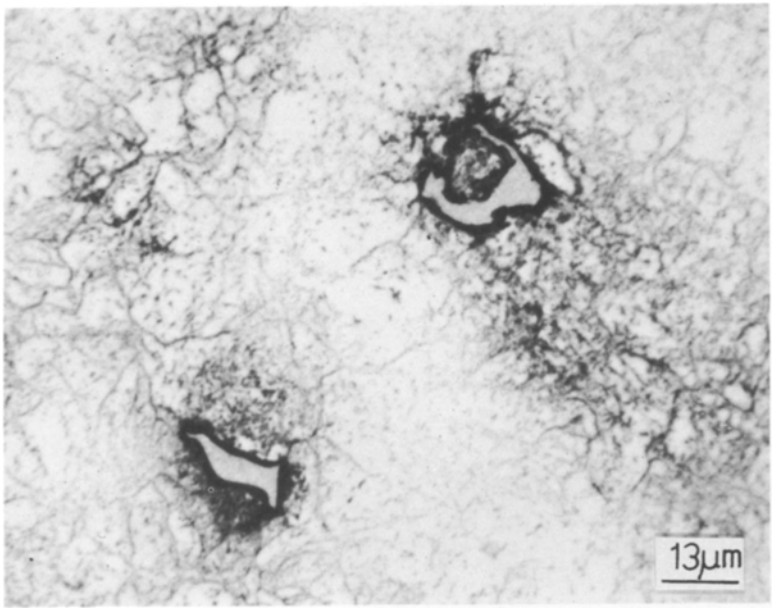

Figure 3 Aged at 705° C for 68 h. Residual carbide with feathery interdendritic precipitate.

ingly evident with rising temperature, Figs. 4 and 6. A change to a blocky morphology was visible under the scanning electron microscope (SEM), Fig. 5, and at later stages under optical microscopy, Fig. 6. Relatively large blocky carbides grew readily in the grain boundaries prior to the morphology change, Fig. 7. The cause of this was the large mismatches which may be accommodated in these regions, and also the increased growth rate due to the increased diffusion rates along grain boundaries.

The second response also occurred in association with the grain boundaries. The dark phase observed in the unaged material grew on ageing, and lamellae were resolved under SEM, Fig. 7. As the ageing temperature was revised so the interlamellar spacing increased, Figs. 8 and 9, in similar fashion to that reported by Weeton and Signorelli [6].

Increasing temperature gave rise to other changes in the microstructure. Within the matrix, the precipitate tended to grow along well-defined

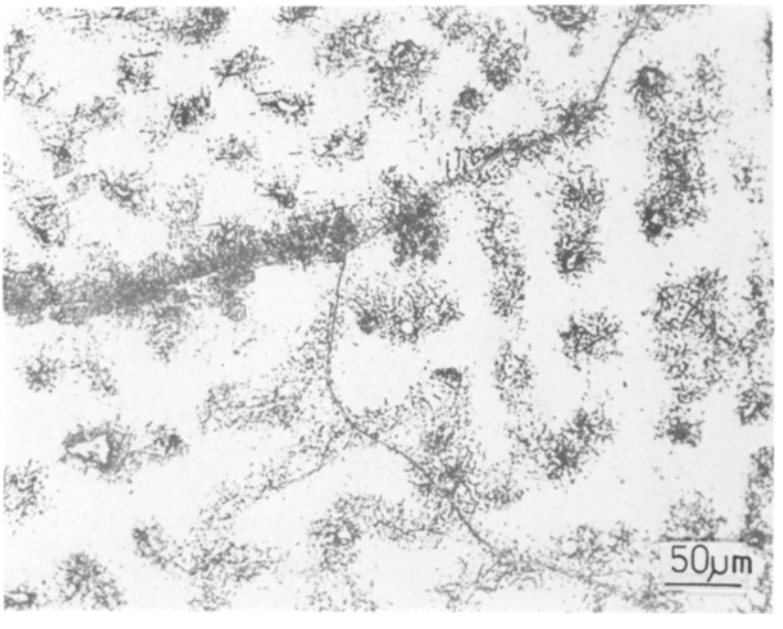

Figure 4 Aged at 980° C for 5 h. Residual carbide with feathery interdendritic precipitate and lamellar structure at grain boundary.

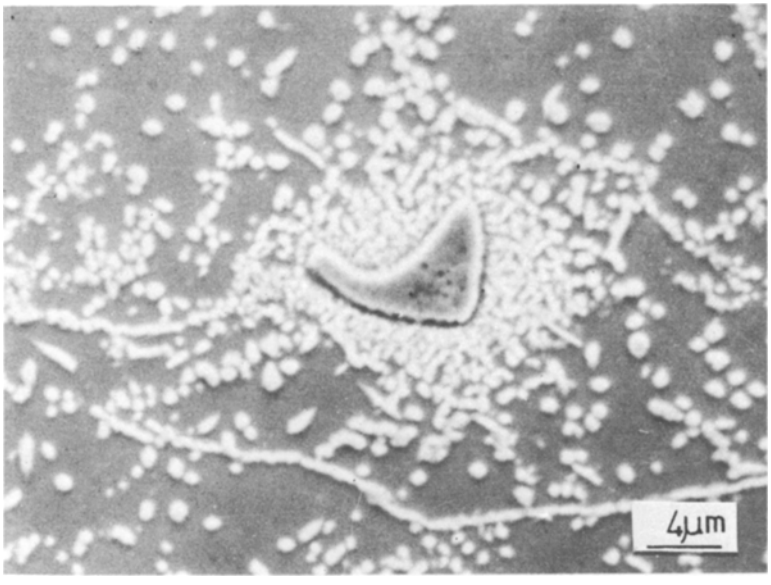

Figure 5 Aged at 925° C for 5 h. SEM picture showing residual carbide particle surrounded by blocky precipitate.

planes in a Widmanstätten type morphology, Figs. 4 and 6. Ostwald ripening, or particle coarsening, was also apparent on extended ageing. Both of these reduced the total free energy of the system, affecting the strain and interfacial components, respectively.

At higher ageing temperature only small amounts of the lamellar phase were present during the early stages of treatment, before spheroidization and agglomeration took place, Fig. 9. Dissolution occurred at 1150° C and over.

3.3. Electron microscopy

3.3.1. Precipitation in the matrix (< 925° C)

The production solution treated material exhibited long stacking faults and slightly dissociated dislocations in the f c c cobalt (α) matrix. The former were shown to be intrinsic by the method devised by Gevers *et al.* [21].

On ageing at 760° C the stacking fault density increased prior to precipitation, which was seen to occur after 2 h. Discrete particles appeared in

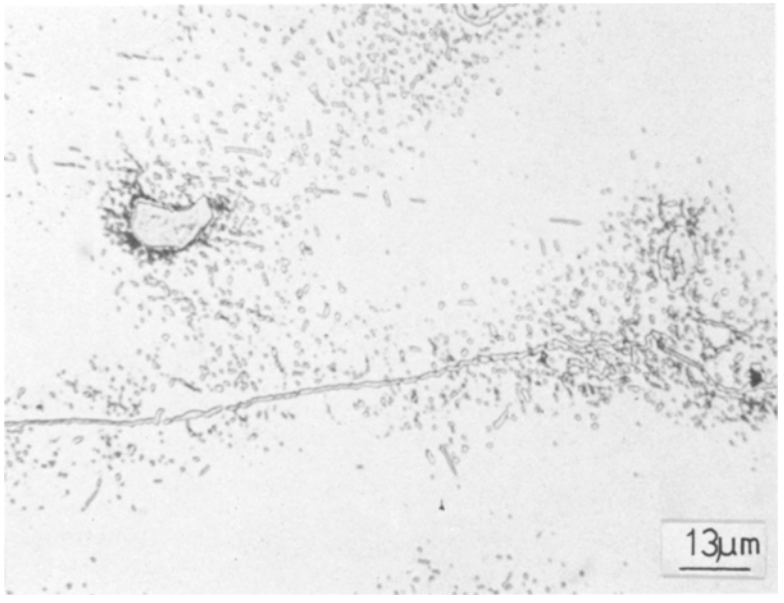

Figure 6 Aged at 1095° C for 1 h. Residual carbide particles with blocky precipitate around them and in grain boundary.

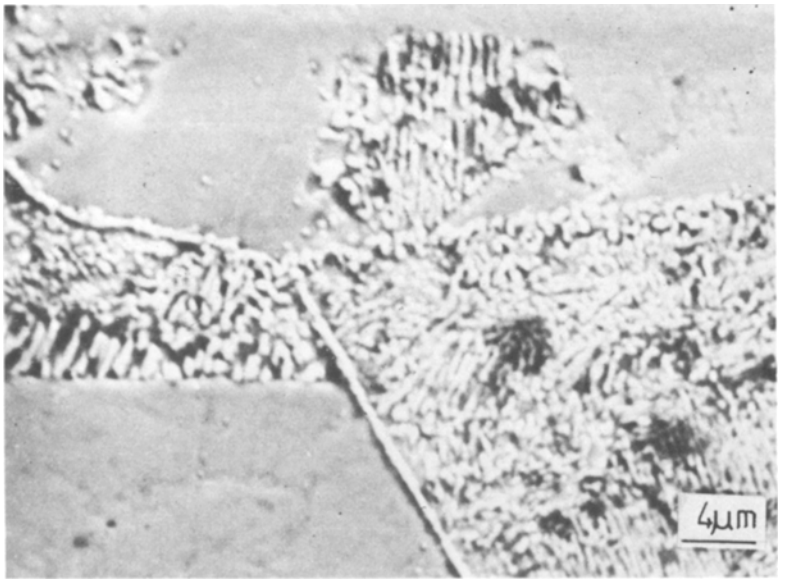

Figure 7 Aged at 760° C for 5 h. SEM picture showing lamellar structure at grain boundary.

association with small stacking faults, Figs. 10 and 11.

When the dark field image of the $M_{23}C_6$ carbide was projected the precipitates were clearly visible. Extended ageing produced an increase in both the fault and precipitate density, but not extensive growth of existing faults took place. The dense tangles shown in Fig. 10 made the determination of the nature of the stacking fault very difficult, and the Burgers vectors of the bounding partial dislocations were not ascertained. However, intrinsic stacking fault was considered probable since this type of lattice defect changes the f c c stacking to that of the h c p (ϵ) allotrope.

Wherever precipitates were abundant enough to produce their own electron diffraction pattern, a close connection with the cobalt matrix was clearly evident, Fig. 12a and b. A cube/cube relationship existed between the two lattices so that:

$$\{1\,1\,1\}_{\mathrm{fcc\ Co}} \| \{1\,1\,1\}_{M_{23}C_6}$$

$$\langle 1\,1\,0\rangle_{\mathrm{fcc\ Co}} \| \langle 1\,1\,0\rangle_{M_{23}C_6}$$

$$\{1\,0\,0\}_{\mathrm{fcc\ Co}} \| \{1\,0\,0\}_{M_{23}C_6}.$$

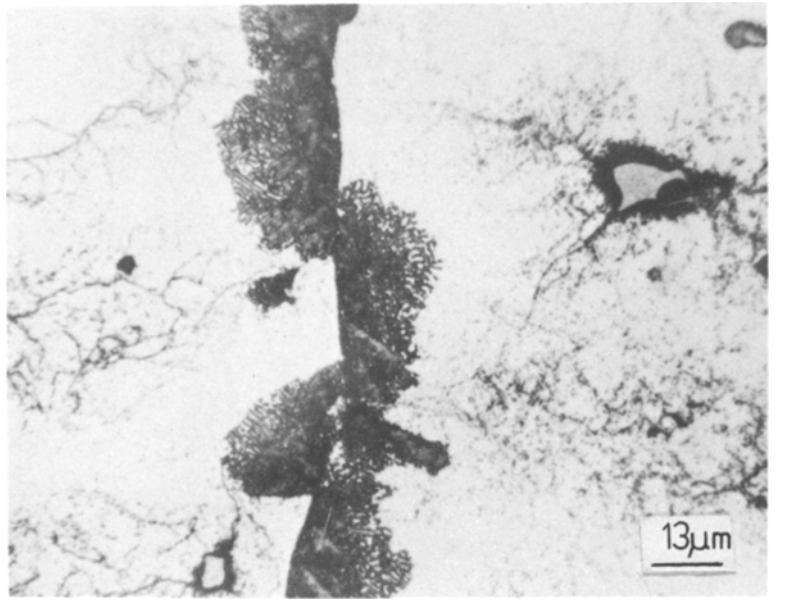

Figure 8 Aged at 870° C for 2 h. Coarser lamellar structure in grain boundary showing the S-shape configuration.

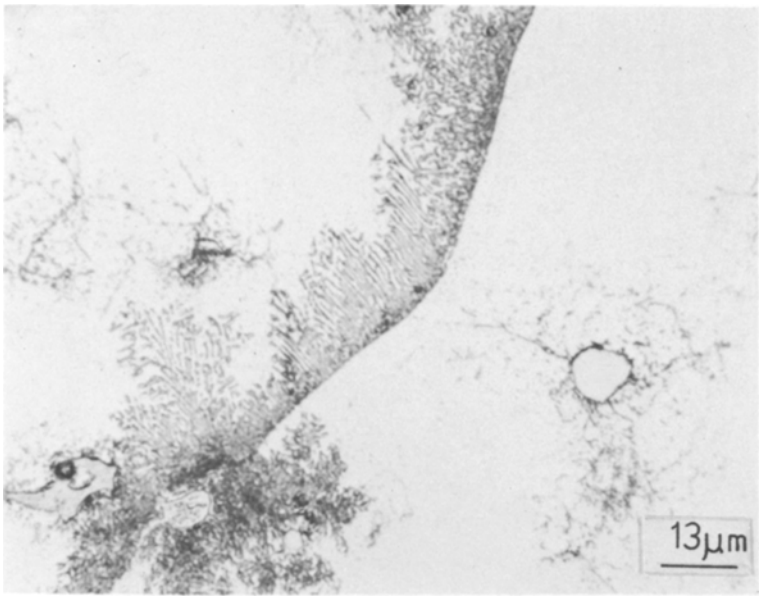

Figure 9 Aged at 980° C for 0.5 h. Coarse lamellar structure in grain boundary.

The proposal of a mechanism for the nucleation and growth of the $M_{23}C_6$ precipitation must be carefully considered, since several possibilities exist. Various studies have observed the phenomenon of precipitation in association with stacking faults in cobalt, aluminium, nickel and iron based alloys, although a variety of mechanisms operated.

Silcock and Tunstall [22] put forward the mode of repeated nucleation on Frank partial dislocations of NbC in austenitic stainless steels. The carbides nucleate in the Frank bounding intrinsic stacking fault, which is formed by the dissociation of a sessile unit dislocation:

$$\tfrac{1}{2}[1\,1\,0] \rightarrow \tfrac{1}{3}[1\,1\,1] + \tfrac{1}{6}[1\,1\,\bar{2}] \qquad (1\,1\,1).$$

UNIT FRANK SHOCKLEY

As the carbide grows, vacancy emission by the movement of the Frank partial by climb, enables the mismatch to be accommodated, so that the dislocation expands between the particles, eventually engulfing them in stacking fault. The process is then repeated. A similar mode was observed by Kotval [23] in a nickel based alloy, where NbC precipitates were again associated

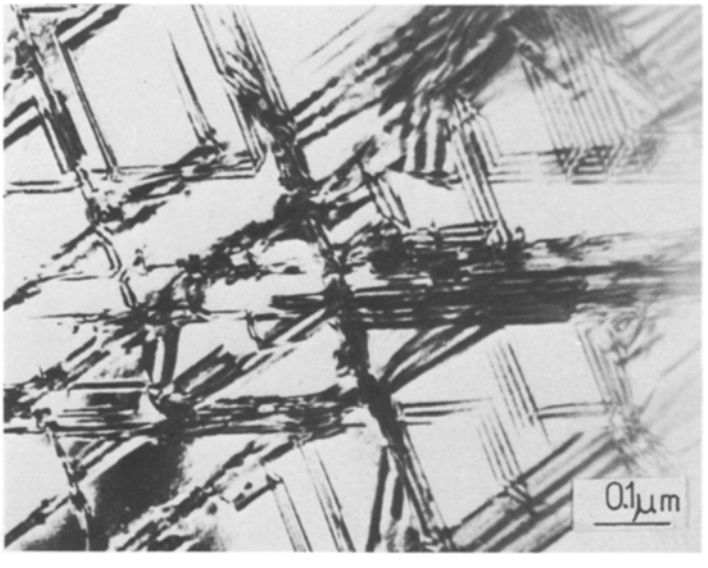

Figure 10 Aged at 760° C for 5 h. TEM picture showing precipitate particles associated with stacking faults.

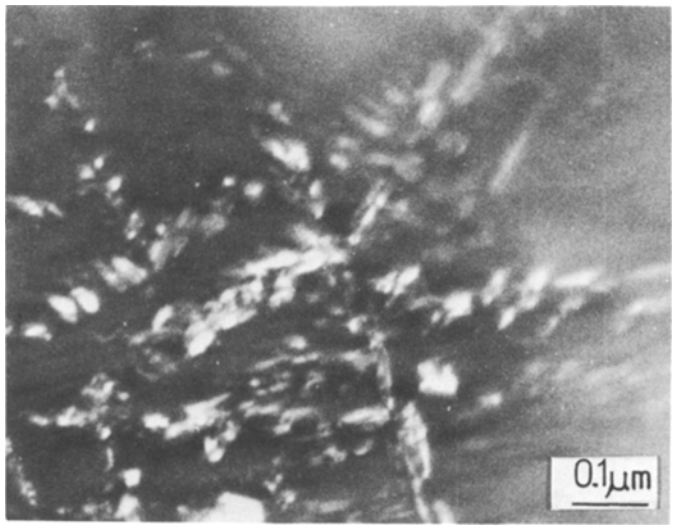

Figure 11 As Fig. 10 – dark field image showing the precipitate particles.

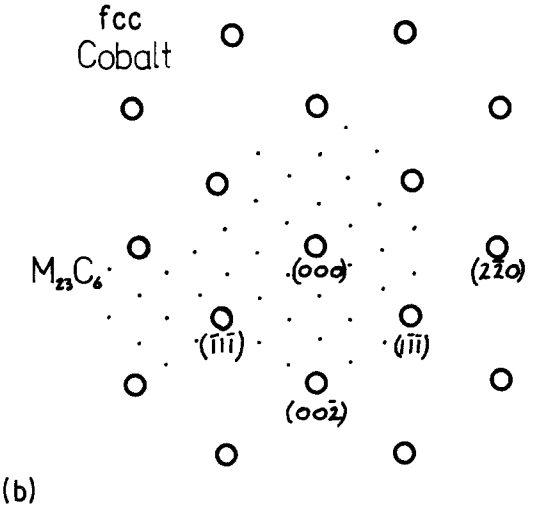

Figure 12 (a) Electron diffraction pattern of structure shown in Figs. 10 and 11. The major spots are fcc cobalt matrix and the fine spots are $M_{23}C_6$. (b) Interpretation of Fig. 12a showing cube/cube relationship between the matrix and $M_{23}C_6$ precipitate.

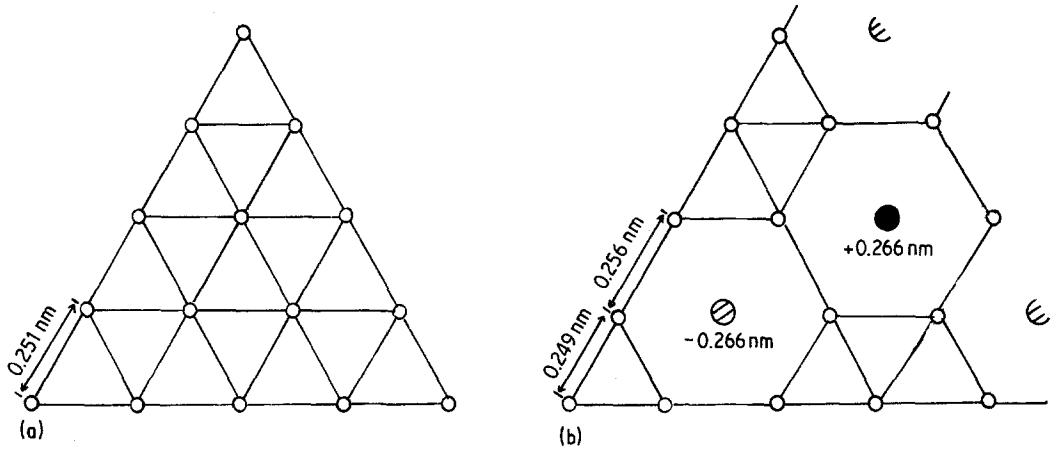

Figure 13 (a) Close packing of cobalt atoms on {1 1 1} and (0 0 0 1). (b) $M_{23}C_6$ atom packing on {1 1 1}.

with extrinsic stacking fault. However, it was put forward [23] that cobalt base alloys, having such a low stacking fault energy, would dissociate with the reaction:

$$\tfrac{1}{2}[1\,1\,0] \rightarrow \tfrac{1}{6}[2\,1\,1] + \tfrac{1}{6}[1\,2\,1] \quad (1\,1\,1).$$

UNIT SHOCKLEY SHOCKLEY

This results in intrinsic stacking fault. The Shockley partials move by glide, and therefore the emission of vacancies through climb is not involved as with Frank partial movement. Repeated nucleation on the Shockleys might occur but the partial dislocation would be pinned by the precipitate and the driving force behind the formation of hcp cobalt would be too weak to prove effective. Any mismatch could not be accommodated easily, although this has been shown to be slight (Section 3.3.2).

Precipitation of $M_{23}C_6$ on Shockley partials has been suggested by Beckitt and Clark [24]. A long thin lath was produced by the nucleation and growth of the carbide on one, pinned Shockley, and the repulsion of the other partial dislocation.

However, the two mechanisms described would have shown various microstructural features which were not observed. Firstly, wide contrast would have been visible at the unit dislocation prior to dissociation. Secondly precipitation on the bounding partial would also give it a ragged appearance, and finally a string-like morphology of growth resulting from the movement of the partial would be apparent.

In some AlCuLi alloys [25] at low supersaturations, the formation of the T_1 (Al_2CuLi) phase was preceded by the production of stacking fault. It was found that copper and lithium enrichment of the intrinsic stacking fault took place followed by precipitation of the hexagonal T_1-phase. Since the fault was also hexagonal in structure, a reduction in interfacial energy was present.

In the system under consideration here, the carbide had a complex fcc, and not hcp, crystal structure. However, a study of the possible mismatch showed that the fcc cobalt {1 1 1} and hcp cobalt {0 0 0 1} planes were identical in both atomic spacing and arrangement, Figs. 13a and b. Therefore the $M_{23}C_6$ {1 1 1} planes would not experience any change when precipitating on intrinsic stacking faults.

Preferential diffusion to the faulted regions, known as "Suzuki segregation", was initially proposed as the mechanism for NbC precipitation prior to repeated nucleation on Frank partials [26–28]. The equilibrium concentration of solute would be different due to the difference in crystal structure. The diffusion rate would increase with decreasing atomic density. However, in the case of cobalt, the two allotropic forms are very similar in crystallographic properties. The space packing of hcp (ϵ) = 73.65% as opposed to 74.05% for the fcc (α) from the data published [29]. The metal atom volume was calculated giving values of 1.1103×10^{-2} nm^3 (11.103 Å^3)/atom and 1.113×10^{-2} nm^3 (11.13 Å^3)/atom, respectively. These figures were dependent upon the accuracy of the crystallographic data, in which there was considerable variance [29]. Both of the results implied that the hcp form would aid the diffusion of solute atoms, but only slighly. No direct data were available on the solubilities of chromium

and molybdenum in the two types of cobalt lattice.

Jacobssen [30] proposed the preferential segregation of the solute (Ti) atoms to faulted regions as the reason for the precipitation of TiC on stacking faults in two CoTiC alloys, heat treated at 700° C → 750° C.

The observations made in this study inferred a similar mode of precipitation. The absence of thick dislocation contrast, the predominance of stacking fault networks prior to precipitation and the uniform appearance of partial dislocations discouraged the idea of repeated nucleation. The random carbide distribution on the stacking fault and the absence of precipitate-free zones, however, did promote the mechanism of solute (Suzuki) segregation as the mode of nucleation.

The discrepancy between these and the results obtained on CoCrC alloys [31, 32] must be attributed to the increased complexity of the system under study. The reduced chromium content and the absence of molybdenum would reduce the tendency to form h c p cobalt and network of intrinsic stacking fault.

3.3.2. Precipitation in the matrix (> 925° C)

When aged at temperatures above 925° C, the mechanism of precipitation within the grains had changed, together with a reduction in the number of stacking faults present. This demonstrated the increasing thermodynamic stability of the f c c cobalt lattice.

Polyhedral precipitates of $M_{23}C_6$ nucleated and grew on dislocations, but no association with the few stacking faults present was observed, Fig. 14. The cube/cube relationship between the carbides and matrix was again evident.

With extended ageing times and increased ageing temperatures, growth of the polyhedral particles occurred, Fig. 15, together with the appearance of laths. Electron diffraction patterns indicated carbide growth in {1 1 1} planes predominantly. Calculation of the atomic packing of the various planes in the carbide were made using information supplied by K. W. Andrews in [24], based on Goldschmidt's [20] model and using a lattice parameter of 1.065 nm. It was found that the {1 1 1} $M_{23}C_6$ and {1 1 1} f c c cobalt planes exhibited the closest matching and substantiates the observations made, Fig. 13.

It was therefore apparent that growth occurred mainly on the {1 1 1} planes. After extensive ion beam thinning on one specimen, a primary residual carbide became visible, and again the selected area diffraction pattern indicated that the bounding surfaces were the {1 1 1} planes.

The change in morphology seen under optical microscopy may be explained as simply a result of the size of the precipitate and the increasing mismatch with the matrix, highlighted by the presence of profuse stacking fault at the interface, Fig. 15. The large grain size prohibited detailed examination of the grain boundaries, but when found, the grain boundary carbides showed no difference from those in the matrix apart from their size.

The difference in nucleation mechanism of NbC from stacking faults to dislocations in austenitic stainless steels was attributed to the enhanced solute diffusion rates which existed at the higher temperatures [26–28]. This was a factor in this study, but in addition, the increased thermodynamic stability of the f c c lattice and subsequent reduced energy for stacking fault formation must have had a significant effect.

3.3.3. The grain boundary lamellar phase

The extensive investigation made by Weeton and Signorelli [6] did not establish a correlation between alloy composition and isothermal temperature, and in addition the nature of the phase was not clarified. The possibility existed that a discontinuous/cellular reaction, and not a eutectoid reaction from solid solution, was taking place. Electron microscopy was required to clarify the situation. Previous ageing studies in which the lamellar morphology had been present unfortunately did not report any transmission electron microscopy (TEM) observations [14].

Despite the large grain size of the specimens, grain boundaries were found in thin sections of various heat treatments. The lamellar morphology was clearly evident after a relatively low temperature age (760° C), Fig. 16. Electron diffraction patterns showed that the precipitating $M_{23}C_6$ carbide exhibited a cube/cube relationship with the top grain in Fig. 16. This had been indicated by the appearance of the stacking fault between the lamellae. No h c p (ϵ)-phase was found, and therefore a discontinuous reaction has taken place and not a eutectoid decomposition.

Some factors of the growth of the lamellar structure were seen under optical microscopy,

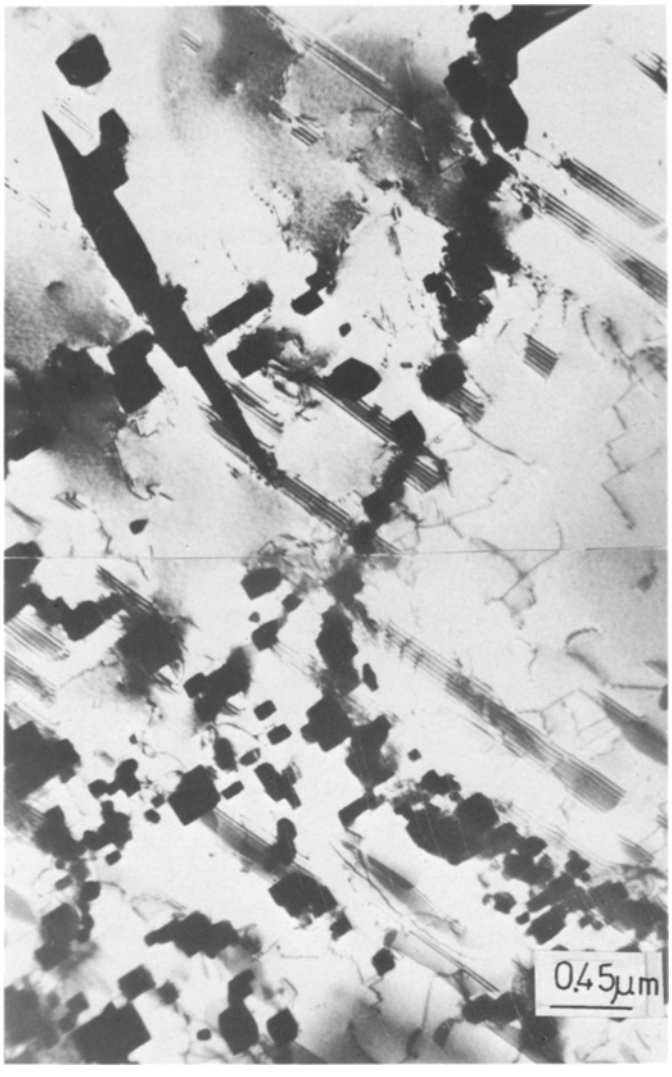

Figure 14 Aged 1040° C for 0.5 h. TEM picture showing grain boundary precipitation of cuboid particles. Note parallel orientation typical of cube/cube relation with matrix.

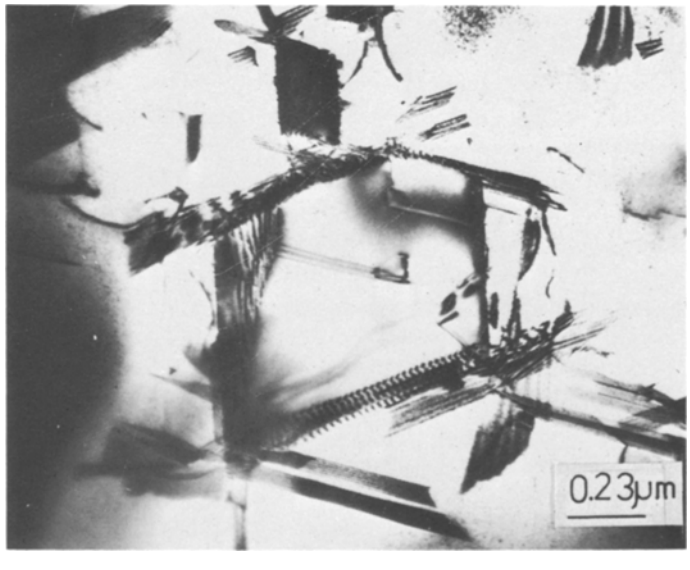

Figure 15 Aged at 1040° C for 16.5 h. TEM picture of large polyhedral precipitate particle with stacking faults in the interface with the matrix.

Figure 16 Aged at 760° C for 5 h. TEM picture of lamellar precipitation and stacking faults at grain boundary. Note bowing out of lamellar region into neighbouring grain.

Figs. 8 and 9. All three types of morphology, single seam, double seam and S-type [33], were evident in many of the ageing operations, although many grain boundaries were free of lamellae. In their review paper, Williams and Butler [34] concluded that it was the characteristics of each individual grain boundary which determined both the morphology and the growth of the cells.

However, two mechanisms have been proposed for the initiation of discontinuous reactions [35, 36]. The former described a mechanism dependent upon heterogeneous grain boundary precipitation, the latter upon grain growth and recrystallization. Bauman *et al.* (33) concluded that the temperature of the transformation as well as the precipitate characteristics determined the mode of cell formation. At temperatures above the crystallization temperature, single seam morphologies predominated due to grain growth, and at temperatures below, double seam and S-type morphologies were evident, as previously reported [35, 36].

In this study, therefore, boundary migration would be expected to control the cell morphology (melting temperature (K)/2 = 660 to 680° C), and the grain boundaries were seen to be bowing out in front of the lamellae, Figs. 16 and 17. The presence of the blocky carbides in the grain boundaries might have promoted the S-type and double seam morphologies, and therefore the precise mechanism of initiation and growth was unclear. The concurrent continuous precipitation within the

Figure 17 Aged at 760° C for 5 h. TEM picture showing lamellar region bowing out into adjacent grain.

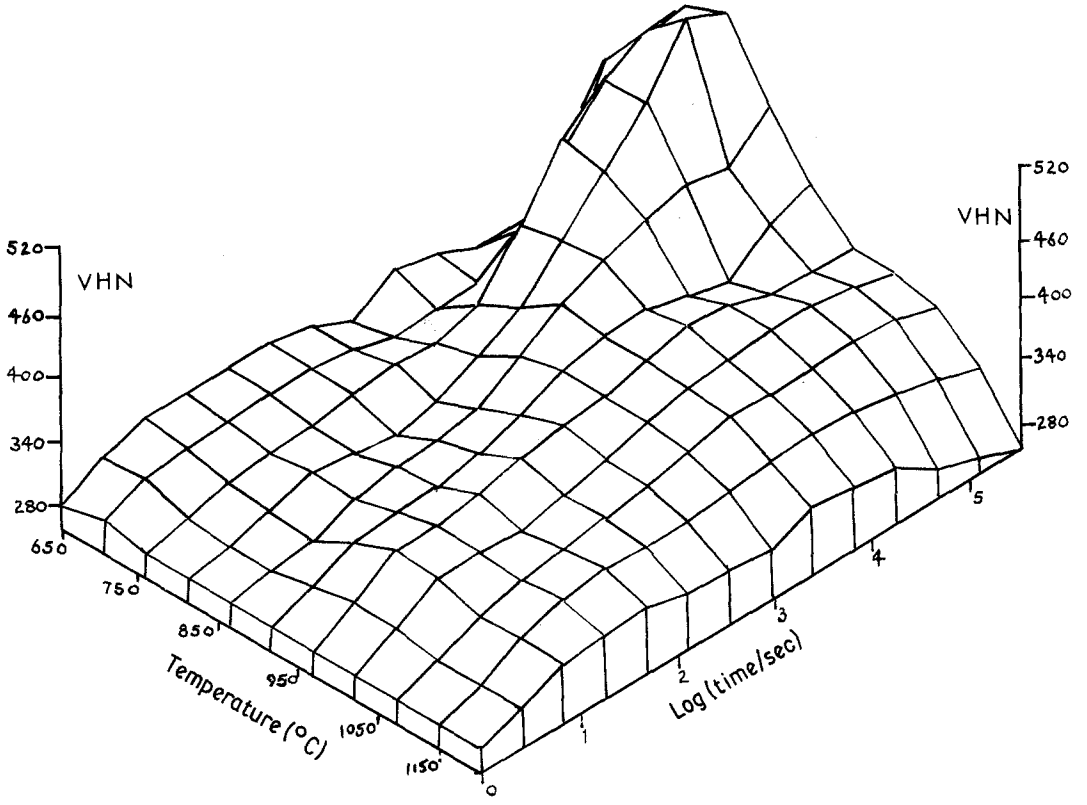

Figure 18 Three-dimensional plot relating age hardening to time and temperature of ageing showing large increase in hardness in temperature range 750 to 800° C after times of 1.5 to 15 h.

matrix would have reduced the chemical driving force for the discontinuous reaction due to solute depletion. This was evident at the higher ageing temperatures when the increased solute diffusion rates in the matrix precluded the necessity for the formation of lamellae.

3.3.4. Age-hardening characteristics

Pyramidal Vickers hardness tests were carried out on the metallographically prepared specimens, an average result taken from at least six readings, due to the large grain size of the material. Microhardness tests were invalid due to the presence of a thin work-hardened layer on the surface.

The results have been plotted three-dimensionally by computer and are shown in Fig. 18. It was clear that substantial hardening occurred at $\sim 800°$ C, after extensive times (> 24 h). A series of tensile tests was performed on specimens aged at 815° C in order to investigate fully any improvement in mechanical properties associated with this hardening response. From the results shown in Fig. 19 it was apparent that no commercial benefit was forthcoming from this type of heat treatment since the ductility (per cent elongation) was drastically reduced as soon as carbide precipitation appeared. This is unacceptable by BS 3521.

The high hardnesses recorded resulted from the dispersion of carbide along the stacking faults, whereas the dislocation nucleated precipitate at higher temperatures had only a minimal effect. This concurred with the observations made on some austenitic stainless steels [37, 38]. It was suggested that both the carbide and the stacking fault contributed to the strengthening [38], the networks of the latter acting as barriers to dislocation movement in a similar fashion to grain boundaries. The rapid work hardening rate of the material can be attributed to the formation of dissociated dislocations which hinder cross slip and climb and therefore postpone the onset of work softening.

4. Conclusions

The precipitation processes on ageing the production solution treated CoCrMoC alloy can be described.

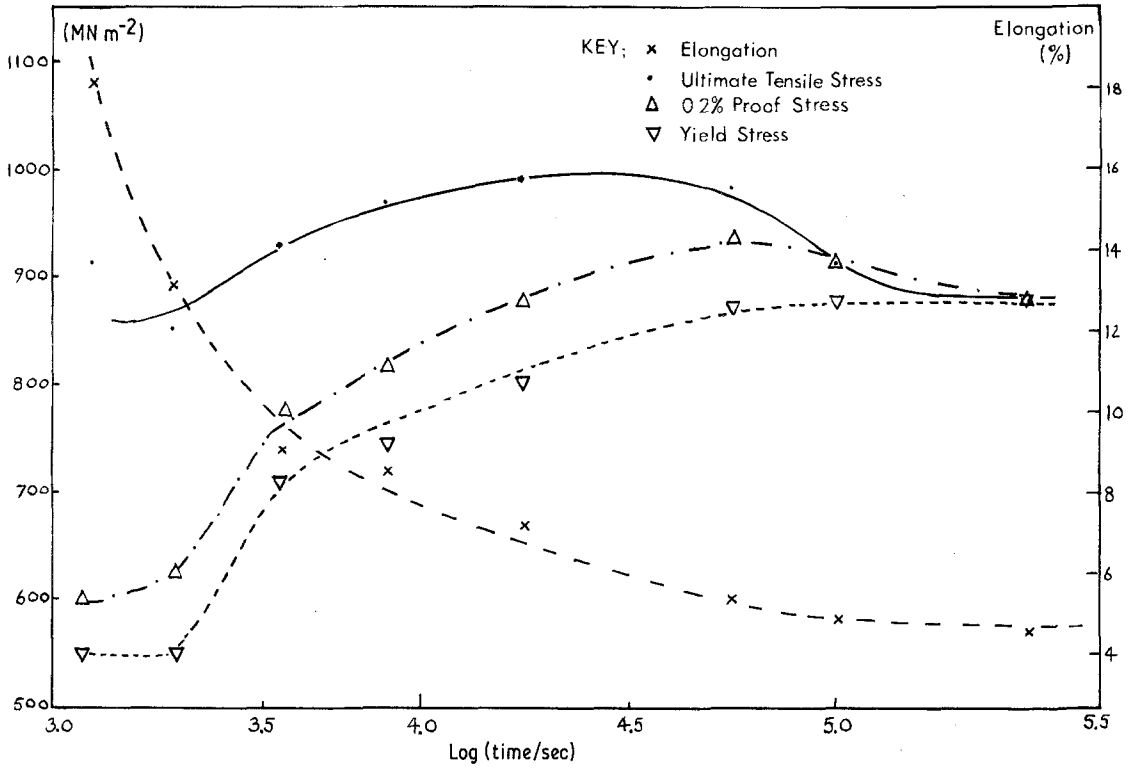

Figure 19 Tensile properties of production solution heat treated material aged at 815° C as a function of ageing time.

At low (< 900° C, > 650° C) ageing temperatures, the $M_{23}C_6$ carbide nucleated and grew in association with stacking fault within the f c c cobalt matrix. The mechanism was probably not through repeated nucleation on particles, but rather by Suzuki segregation. In order to facilitate the precipitation of $M_{23}C_6$, retarded by the low supersaturation and the limited solute diffusion within the matrix, a discontinuous reaction occurred at the grain boundaries which resulted in the appearance of a lamellar morphology. The grain boundaries also acted as nucleation sites through their enhanced diffusion rates and the ability to accommodate relatively large mismatches.

At ageing temperatures in excess of ~ 900° C, the precipitation mechanism of the carbide changed to nucleation on dislocations. Growth occurred on distinct crystallographic planes, nominally the 1 1 1 of both $M_{23}C_6$ and the cobalt matrix. In all instances a cube/cube relationship existed between the two lattices. The change in nucleation mode was a result of the increased stability of the f c c cobalt allotrope and the enhanced diffusion rates associated with the increased ageing temperature. Some lamellae were formed at these higher temperatures, but their extent and growth were limited.

Despite increases in hardness and strength after some of the ageing operations, notably at 815° C, no benefit in mechanical properties was realised due to the rapid decreases in ductility associated with these treatments.

Acknowledgements

The authors would like to express their gratitude to Dr J. H. Dumbleton and Howmedica International Inc., for the provision of the material and the help and cooperation received. RNJT is also indebted to the Science and Engineering Research Council for the funding of this work. Finally, the authors would like to thank their colleague Dr B. Noble for helpful discussion on the transmission electron microscope results.

References

1. G. W. MEETHAM, *Met. Mater. Technol.* 14 (1982) 387.
2. C. T. SIMS and W. C. HAGELS, "The Superalloys" (J. Wiley and Sons, New York, 1972) p. 145.
3. C. P. SULLIVAN, J. D. VARIN and M. J. DONACHIE Jr, *Met. Eng. Quart.* 9 (1969) 16.
4. F. J. CLAUSS and J. W. WEETON, NACA TN 3107

(1954).
5. *Idem*, NACA TN 3108 (1954).
6. J. W. WEETON and R. A. SIGNORELLI, NACA TN 3109 (1954).
7. F. J. CLAUSS, F. B. GARRETT and J. W. WEETON, NACA TN 3512 (1955).
8. N. J. GRANT, *Trans. ASM* **39** (1947) 281, 335.
9. N. J. GRANT and J. R. LANE, *ibid.* **41** (1949) 95.
10. J. R. LANE and N. J. GRANT, *ibid.* **44** (1952) 113.
11. J. W. WEETON and R. A. SIGNORELLI, *ibid.* **47** (1955) 815.
12. A. J. T. CLEMOW and B. L. DANIELL, *J. Biomed. Mater. Res.* **13** (1979) 265.
13. E. E. FLETCHER and A. R. ELSEA, *Trans. AIME* **191** (1955) 897.
14. J. B. VANDER SANDE, J. R. COKE and J. WULFF, *Met. Trans. A.* **7A** (1976) 389.
15. M. J. DONACHIE, Jr and O. H. KRIEGE, *J. Mater.* 7 (1972) 264.
16. S. YUKAWA and K. SATO, *Trans. JIM* 9 (1968) (Supplement) 680.
17. B. LUX and W. BOLLMANN, *Cobalt* **33** (1961) 32.
18. J. M. DRAPIER, V. LE ROY, C. DUPONT, D. COUTSOURADIS and L. HABRAKEN, *ibid.* **41** (1968) 199.
19. M. J. WOULDS and T. R. CASS, *ibid.* **42** (1969) 3.
20. H. J. GOLDSCHMIDT, *JISI* **160** (1948) 345.
21. R. GEVERS, A. ART and S. AMELINCX, *Phys. Status Solidi* **3** (1963) 1563.
22. J. M. SILCOCK and W. J. TUNSTALL, *Phil. Mag.* **10** (1964) 361.
23. P. S. KOTVAL, *Trans. AIME* **242** (1968) 1651.
24. F. R. BECKITT and B. R. CLARK, *Acta Metall.* **15** (1967) 113.
25. B. A. NOBLE and G. E. THOMPSON, *Met. Sci. J.* 8 (1972) 167.
26. J. S. T. VAN ASWEGAN, R. W. K. HONEYCOMBE and D. H. WARRINGTON, *Acta Metall.* **12** (1964) 1.
27. J. M. SILCOCK, *JISI* **201** (1963) 409.
28. P. W. TEARE and N. T. WILLIAMS, *ibid.* **201** (1963) 125.
29. "The Cobalt Monograph", edited by Centre d'Information du Cobalt, Brussels (1960).
30. B. E. JACOBSSEN, *Met. Trans. A.* **11A** (1980) 1156.
31. P. A. BEAVEN, P. R. SWANN and D. R. F. WEST, *J. Mater. Sci.* **13** (1978) 691.
32. *Idem, ibid.* **14** (1979) 334.
33. S. F. BAUMAN, J. MICHAEL and D. B. WILLIAMS, *Acta Metall.* **29** (1981) 1343.
34. D. B. WILLIAMS and E. P. BUTLER, *Int. Met. Rev.* **26** (1981) 153.
35. K. N. TU and D. W. TURNBULL, *Acta Metall.* **15** (1967) 369.
36. R. A. FOURNELL and J. B. CLARK, *Met. Trans.* 3 (1972) 2757.
37. R. D. NAYBOUR, *JISI* **204** (1966) 1200.
38. M. J. HARDING and R. W. K. HONEYCOMBE, *ibid.* **204** (1966) 259.

Received 1 March
and accepted 16 March 1983